ACS Photonics

Letter

pubs.acs.org/journal/apchd5

Size-Dependent Coherent-Phonon Plasmon Modulation and Deformation Characterization in Gold Bipyramids and Nanojavelins

Matthew S. Kirschner,[†,‡] Clotilde M. Lethiec,[†] Xiao-Min Lin,[‡] George C. Schatz,[†] Lin X. Chen,[†,§] and Richard D. Schaller*[,†,‡]

[†]Department of Chemistry, Northwestern University, 2145 Sheridan Road, Evanston, Illinois 60208, United States

[‡]Center for Nanoscale Materialsand [§]Chemical Sciences and Engineering Division, Argonne National Laboratory, 9700 Cass Avenue, Argonne, Illinois 60439, United States

Supporting Information

ABSTRACT: Localized surface plasmon resonances (LSPRs) arising from metallic nanoparticles offer an array of prospective applications that range from chemical sensing to biotherapies. Bipyramidal particles exhibit particularly narrow ensemble LSPR resonances that reflect small dispersity of size and shape but until recently were only synthetically accessible over a limited range of sizes with corresponding aspect ratios. Narrow size dispersion offers the opportunity to examine ensemble dynamical phenomena such as coherent phonons that induce periodic oscillations of the LSPR energy. Here, we characterize transient optical behavior of a large range of gold bipyramid sizes, as well as higher aspect ratio nanojavelin ensembles with specific attention to the lowest-order acoustic phonon mode of these nanoparticles. We report coherent phonon-driven oscillations of the LSPR position for particles with resonances spanning 670 to 1330 nm. Nanojavelins were shown to behave similarly to bipyramids but offer the prospect of separate control over LSPR energy and coherent phonon oscillation period. We develop a new methodology for quantitatively measuring mechanical expansion caused by photogenerated coherent phonons. Using this method, we find an elongation of approximately 1% per photon absorbed per unit cell and that particle expansion along the lowest frequency acoustic phonon mode is linearly proportional to excitation fluence for the fluence range studied. These characterizations provide insight regarding means to manipulate phonon period and transient mechanical deformation.

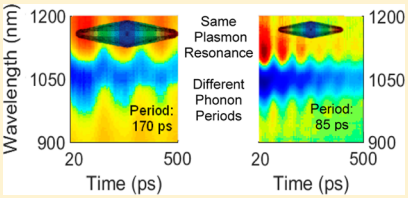

KEYWORDS: *gold nanoparticles, time-resolved spectroscopy, coherent acoustic phonons*

Synthetic control over the size, shape, and composition of metallic nanoparticles affords tunability of localized surface plasmon resonances (LSPRs) from the ultraviolet through the mid-infrared.[1−6] Controlling the LSPR energy facilitates nanoparticle-based applications that range from use as SERS substrates[7−11] and chemical/biological sensors[7,9−11] to medical therapeutic applications[11−13] and photocatalysis.[14,15] Whereas the large extinction cross sections presented by LSPRs draw interest for applications, ensemble polydispersity represents another key feature as reflected in the LSPR line width. Gold bipyramids exhibit narrow ensemble line widths, largely dominated by homogeneous dephasing[16−19] (especially narrow in comparison to spheres and rods), which reflects the monodispersity of the sample. The comparative homogeneity of the ensemble permits time-dependent, ensemble characterization of coherent acoustic phonon oscillations[17−19] that interestingly yield prominent, periodic shifts of the LSPR energy owing to expansion and contraction of the particles. While other nanostructures can exhibit the same phenomenon, particle size dispersion leads to variation in phonon frequencies causing fast inhomogeneous damping that typically dominates ensemble dynamics.[4−6,20] Several single particle experiments have been performed that circumvent inhomogeneous dephasing.[21−23] At the same time, this approach can impart complexities such as substrate interactions, owing to the requirement that the nanomaterial remains stationary, which can limit the generality of these measurements.

Previously, Pelton et al. examined bipyramids with an LSPR near 700 nm, characterized and also modeled the LSPR oscillations via a parameter-free model.[17] They could separate damping processes related to energy dissipation into solvent (fluidic damping) versus particle-intrinsic damping and found that intrinsic damping was consistent across a range of suspension media. In subsequent work, they generalized this model to include particles with an arbitrarily slender shape and, by characterizing a series of similarly sized particles, argued that damping is a property of material and geometry.[18] Fernandes et al. demonstrated use of bipyramid acoustic phonons to perform mass sensing.[19] Upon growing a thin layer of silver on a gold bipyramid sample they were able to observe a shift in vibrational frequency and correlated the shift to the mass of silver added. Their work also led to observation of higher-order vibrational modes of bipyramids and the characterization of how such higher-order modes changed with the geometric alteration induced by the addition of silver.

Received: February 24, 2016
Published: April 4, 2016

DOI: 10.1021/acsphotonics.6b00136
ACS Photonics 2016, 3, 758−763

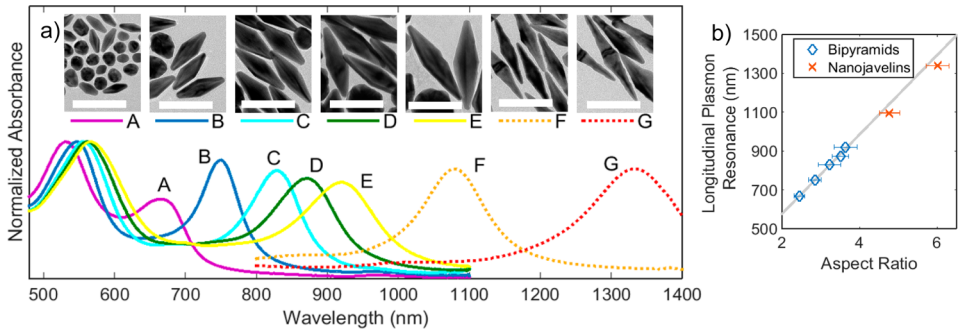

Figure 1. (a; top) Transmission electron microscopy of samples A–G, (bottom) extinction spectra for the indicated samples where solid lines indicate bipyramids (A–E) and dashed lines indicate nanojavelins (F and G). The white scale bars are all 100 nm in length. (b) Position of the longitudinal LSPR vs aspect ratio for samples A–G from panel (a), where the red "x" shapes indicate nanojavelins. The solid line is a linear fit of the five bipyramid samples. Error bars represent standard deviation in ensemble aspect ratio as derived from TEM.

Despite these preceding works, some properties of these coherent phonons remain ambiguous. One such aspect is the fluence- and particle-size-dependent displacement amplitude of the phonon-induced particle deformation in bipyramids, although some studies have measured such for other nanoparticle systems. Hartland measured the expansions of gold nanospheres from coherent acoustic phonons based on shifts in LSPR position obtained from optical transient absorption spectroscopy.[4] He found radial increases around 0.4% for excitation fluxes around 2.5×10^{15} photons/cm^2 of 390 nm pump photons.[4] Other studies utilized X-ray characterizations. Plech observed lattice expansions of <1.2% for laser pump intensities up to near 8×10^{16} photons/cm^2 from a 400 nm source using transient X-ray scattering.[24] Using truncated gold octahedral nanocrystals pumped at a fluence of 4×10^{15} photons/cm^2 from a 800 nm source, expansions of around 0.5% were reported by Clark et al.[25] However, these efforts rely on isotropic systems or complex spectroscopic techniques. A more robust methodology is required to understand acoustic phonon vibration in the ever increasing variety of particle geometries. This need is especially relevant for bipyramids as the most recent synthetic progress is able to produce a wider range of bipyramids with high yield[26,27] as well as nanojavelins, extremely elongated bipyramids with surface plasmon resonances that extend into the near-infrared range.[27]

Here, we report time-resolved spectroscopic measurements and theoretical modeling of a large range of gold bipyramids and nanojavelins with LSPR extinction maxima that range from 670 to 1330 nm. First, we characterize the dependence of coherent phonon dynamics with particle size and aspect ratio, and demonstrate that LSPR position and phonon frequency can independently be varied. Then, we develop a methodology to calculate particle expansion caused by coherent acoustic phonons using transient absorption spectroscopy in conjunction with theoretical modeling. Using this approach, we show that particle expansion is linearly dependent on excitation power with larger particles exhibiting slightly higher relative expansions. Taken together, these results provide a better understanding of how to manipulate phonon dynamics as well as their mechanical impact on nanoparticles.

RESULTS AND DISCUSSION

Independent Manipulation of Plasmon Resonance and Phonon Frequency. Figure 1a shows transmission electron micrographs (TEMs) and extinction spectra (absorption and scattering contribute) for a series of gold bipyramids and nanojavelins (herein referred to as samples A–G) suspended in water with a broad range of LSPR positions, spanning from 670 to 1330 nm. Samples A–E were synthesized following the procedure published by Liu and Guyot-Sionnest,[16] whereas samples F and G were prepared using the procedure outlined by Chateau et al., which results in rougher, sawtooth-like edges.[27] The redder LSPR extinction maxima arise from longitudinal plasmon resonances while features near 550 nm originate from both transverse LSPR modes of the bipyramids/nanojavelins and undesired synthetic side products such as small nanospheres and nanorods.[28] Figure 1b shows that these longitudinal LSPRs depend linearly on aspect ratio, defined as particle length/width, which is consistent with previous measurements.[27]

For each of these samples, we performed broadband transient absorption using a pump wavelength tuned to the LSPR extinction maximum. Despite the differences in the synthesis and surface details, both types of particles present coherent acoustic phonons reflected in their transient absorption spectrum. Figure 2a shows the raw transient absorption spectrum for nanojavelin sample G. We see substantial oscillatory red and blue shifting of the LSPR center wavelength owing to the photoinduced generation of coherent acoustic phonons. Upon elongation, the LSPR broadens and red-shifts to produce an induced absorption feature, as well as a concurrent bleach of the static LSPR position in addition to some evidence of broadening. For all seven samples, and as shown in the inset of Figure 2b, we fit the LSPR oscillatory features and obtained the coherent phonon frequency as well as oscillation quality factors with a procedure detailed in the Supporting Information. We find that phonon periods depend linearly on particle length for bipyramids and nanojavelins, consistent with the lowest-confined acoustic mode.[19] At present, bipyramid syntheses do not permit facile independent tuning of both aspect ratio and length. As a result, adjusting the LSPR yields a concomitant change in the phonon period, which is set by the nanoparticle length. However, it is possible to create nanojavelins with nearly the same length as bipyramids, but significantly different aspect ratios, such as samples D and F. These two ensembles exhibit similar phonon periods of 93 and 85 ps but quite different LSPR resonances of 872 and 1096 nm. Our measurements then demonstrate that, through utilizing nanojavelins, one can further control particle LSPR energy and phonon period.

Mechanical Deformation from Acoustic Phonons. Understanding lattice distortion extent in metal nanoparticles

DOI: 10.1021/acsphotonics.6b00136
ACS Photonics 2016, 3, 758–763

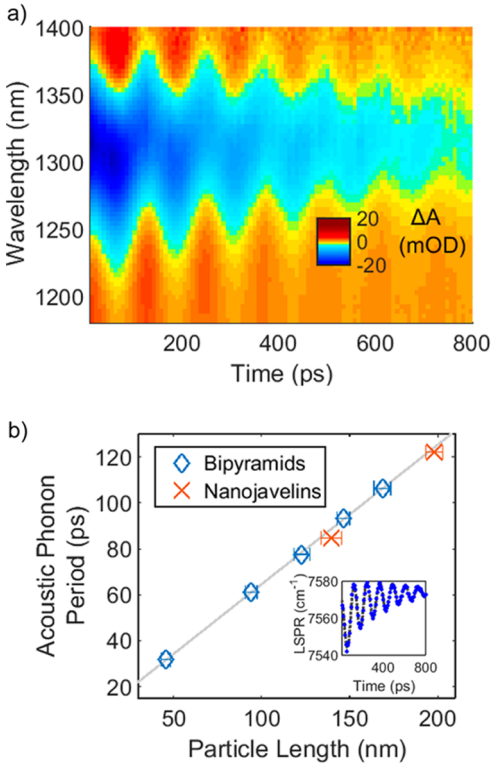

Figure 2. (a) Representative experimental broadband transient absorption dynamics, here for sample G. (b) Particle length vs measured phonon period. This solid line is a linear fit for the five bipyramid samples. Error bars indicate standard deviations in ensemble size. Variation in the phonon period is less than 0.3% so no vertical error bars are included. Inset: LSPR peak center modulation caused by acoustic phonons for the data in panel (a). Experimental data points are shown in blue and the dark gray line arise from fitting to eq 1. Note that the shift in LSPR in the inset relates both coherent phonons and lattice heating. Lattice heating in the samples is discussed in Figure S1 of the Supporting Information.

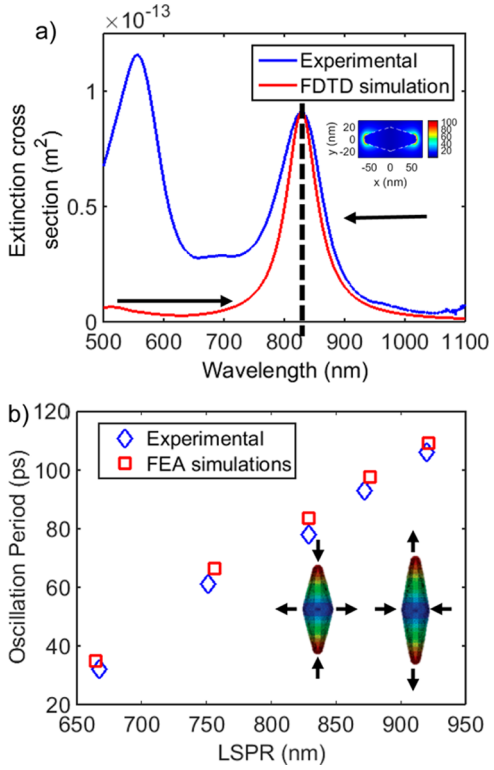

Figure 3. (a) Experimental (in blue, arbitrary unit) absorption spectrum measured on sample C. The absorption spectrum calculated on a gold bipyramid with the same dimensions as sample C is also plotted (in red). The theoretical spectrum displays both the transverse (around 512 nm) and longitudinal (at 829 nm, dash line) plasmon resonances. The experimental transverse plasmon resonance overlaps with the plasmon band from the impurities in the sample. Inset: FDTD simulation of the 2D projected near-field enhancement around the same gold bipyramid as in a, calculated at 829 nm. (b) Measured (blue) and calculated (red) oscillation period of the vibrational mode as a function of the longitudinal plasmon resonance for the five samples of gold bipyramids. Inset: simulated displacement of a bipyramid during acoustic mode oscillation (not at scale).

is generally quite challenging. However, here we develop a technique to quantify the effects of lattice distortions on plasmonic properties. To determine this particle deformation caused by the coherent acoustic phonons we utilized several theoretical tools in conjunction with experimental data. First, we performed finite-difference time-domain (FDTD) simulations using particle dimensions based on TEM images (Table S1) to calculate the extinction spectra of the samples. Figure 3a shows the calculated and experimental optical spectra for sample C. The redder, longitudinal plasmon resonances exhibit good agreement. The calculated higher energy peak, around 512 nm, corresponds to the transverse plasmon mode and is masked in the experimental spectra by the large peak around 555 nm corresponding to the LSPRs of spherical nanoparticles in the sample. These FDTD calculations also provide spatial mapping of the electric field distribution at the particle surface, shown as an inset in Figure 3a of sample C. As expected, the highest field intensity appears close to the tips of the bipyramid, corresponding to the longitudinal plasmon resonance.

We further used finite-element analysis (FEA) to calculate the frequency of the acoustic vibrations associated with the samples. In Figure 3b we show the measured and calculated periods of the acoustic mode as a function of the longitudinal plasmon resonance. The calculated periods closely match those of the measured oscillations with a slight systematic increase.

Figure 4a shows how FDTD and FEA were combined to calculate particle deformation after photoexcitation. Using FEA we were able to determine the direction of the geometric change induced by the acoustic phonon. The LSPR peak shift with expansions of different magnitudes along that phonon mode were then calculated via FDTD. We performed these calculations on bipyramids with a long axis extended in a range of 0.1% to 1% of its original value and contracted along the short axis. Figure 4a shows a rather linear dependence of the LSPR shift as the particle undergoes elongation. These calculations were then used to generate a calibration plot to allow the conversion of peak shift to mode-specific particle elongation.

To relate these calculations to experimental data, we fit the time dependent position of the LSPR after photoexcitation to a function of the following form

$$\omega_\varepsilon(t) = \sum_j \beta_j e^{-t/\tau_{1j}} e^{-(t/\tau_{2j})^2} \sin\left(\frac{2\pi t}{T_j} + \varphi_j\right) + \omega_0 + \alpha e^{-t/\tau_{cool}} \quad (1)$$

This equation includes for a given phonon mode j, the maximum coherent phonon displacement β, homogeneous lifetime τ_1, inhomogeneous lifetime due to nanoparticle

DOI: 10.1021/acsphotonics.6b00136
ACS Photonics 2016, 3, 758−763

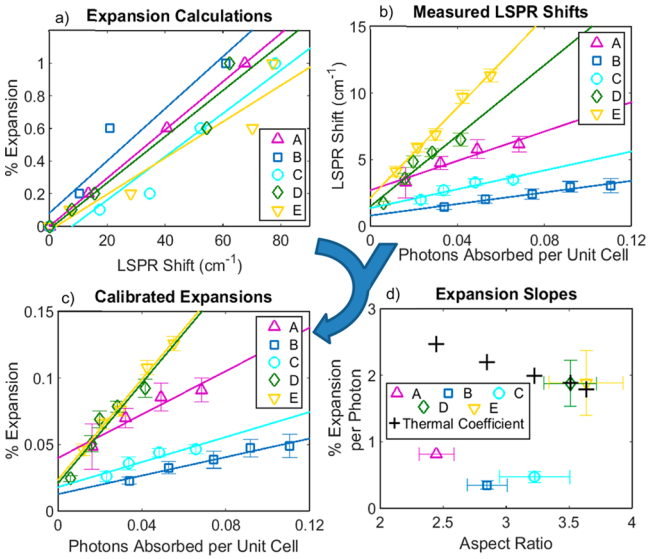

Figure 4. (a) LSPR shift from different particle expansions as estimated from FDTD and FEA simulations. While the particle elongations in these theory calculations are much larger than is observed experimentally, they can be extrapolated to predict dynamics on experimental scales that are not computationally feasible. Since FDTD is highly sensitive to small changes in bipyramid geometry and high-resolution meshing there is some uncertainty in these calculations, on the order of a few wavenumbers. (b) LSPR shifts observed from coherent acoustic phonons normalized for particle size. Unit cells were assumed to be FCC structure (4 atoms per unit cell) and particle absorption cross sections, listed in Table S2, were taken from FDTD calculations. Additional details appear in the Supporting Information. Error bars are the 95% confidence interval from our fitting algorithm. (c) Particle elongation vs photons absorbed per unit cell from the experimental data in b combined with a calibration curve generated from theory results in a. Error bars are the same as those in b. (d) Slopes of linear fits of the data in c along with expected slopes based on the linear thermal expansion coefficient and specific heat of gold. Horizontal error bars are standard deviations in size from TEM images and the vertical error bars represent the uncertainty from the calibration curves (a) calculated from the ratio of the residual sum of squares to the total sum of squares.

polydispersity τ_2, the period of the acoustic vibrations T, and phase shift φ, along with the static LSPR position ω_0, a lattice heating term α, and a lattice cooling lifetime τ_{cool}. Here, a single frequency, the lowest-energy phonon mode, dominates the oscillatory behavior of the LSPR signal and therefore obviates the summation as only one phonon mode is modeled in the fit. Homogeneous quality factors did not exhibit monotonic dependence on particle size, but we suggest these values (which range from roughly 10−30) likely depend on details of the particles such as surface roughness and facet imperfections evident in TEM, as examined and discussed in the Supporting Information (Figures S2−S4) along with information regarding fitting procedures.

Figure 4b shows the coherent phonon-induced shift in the LSPR peak position (β) measured as a function of pump intensity for our bipyramid samples. Note that the extrapolation to zero photons absorbed gives a residual, apparent particle expansion in both theoretical (Figure 4a) and experimental data (Figure 4b). We are unsure why this trend is observed. For the theoretical data it is possibly caused by uncertainty from the high-resolution meshing and prohibitively high precision calculations impedes still smaller-expansion modeling. The low power regime also yields experimentally reduced signal-to-noise. Still, the trend may relay physical meaning. For instance, scattering of hot electrons and higher-energy phonons may cause pre-existing acoustic phonons to enter into phase as phonon injection locking has been reported in other systems,[29] though such a notion requires future research.

Combining the slope information from theory (Figure 4a) and experiment (Figure 4b), we evaluate the power dependence of particle elongation in Figure 4c. This analysis shows that elongation exhibits a fairly linear dependence on excitation intensity, which is consistent with observations for nanospheres using transient X-ray scattering.[24] As can be seen in Figure 4b, LSPR shifts do not exceed 15 cm^{-1} across this range of powers and samples, which we relate to transient particle elongations of less than 0.2%, comparable to what has been reported for nanospheres.[4,24,25] However, we strictly consider coherent, mode-specific expansion whereas prior efforts also included incoherent lattice heating, making it difficult to perform direct comparisons between different reports. We do not expect it is possible to obtain significantly larger changes in particle elongation than those shown in Figure 4 as additional deposited energy from still higher pump intensity likely goes toward rapid melting rather than coherent expansion of the particle.[6,24] In the Supporting Information, we estimate overall changes in particle size from coherent phonons (Figure S7).

Figure 4d shows the slope of percent elongation over photon absorption for the data shown in Figure 4c along with expected slopes from the thermal expansion coefficient of gold.[24] These measured values, when normalized for particle size, exhibit only a slight size dependence with more expansion occurring for larger particles, which could be explained by the longer particles having lower energy phonons. If the bipyramidal phonon modes were populated with a Boltzmann like distribution of energy, higher percentages of the energy would be converted into lower energy phonon modes for these bigger bipyramids. Alternatively, larger bipyramids have higher scattering cross sections. Provided that some of that scattering is inelastic, it will contribute to generation of phonons. However, this effect is expected to be small since scattered photons impart significantly less energy than absorbed photons and the scattering cross section is on the same order of magnitude as the absorption cross sections. Although these differences exist, the expansion per photon absorbed is on the same order of magnitude across the examined size range, which indicates that size dependent effects on elongation are weak. Our measurements are also on the same order as estimated from the thermal expansion coefficients of gold which are dependent on the excitation wavelength with more expansion expected for higher energy photons. This similarity is surprising as the experimental data reflects coherent phonons which constructively interfere, whereas thermal expansion is an incoherent process which also involves destructive interference. Likely, only a small percentage of the absorbed energy goes into these coherent acoustic phonon modes and other heat dissipation pathways are also quite important. These dissipation pathways could be further explored using the analysis developed by Crut and his co-workers which could provide added insight into the size dependence of the expansion per photon absorbed.[19,30,31] It is also worth noting that, based on a cursory pump wavelength dependence study, we anticipate more particle expansion per photon for higher energy photons that can generate additional phonons.

DOI: 10.1021/acsphotonics.6b00136
ACS Photonics 2016, 3, 758−763

In conclusion, we demonstrated that coherent acoustic phonons in nanojavelins exhibit similar size dependent trends as bipyramids providing a method to separately control LSPR position and phonon frequency. Additionally, by using theoretical tools and transient absorption spectroscopy, we show it is possible to quantify particle expansion from photogenerated coherent acoustic phonons which has a linear power dependence that slightly increases with particle size. This information provides a guide for designing particles with tunable LSPR as well as understanding the resulting mechanical response to photoexcitation. Future work could include using these design principle to create gold bipyramids with low frequency phonons excited by convenient wavelengths for mass sensing applications or utilizing the ability to measure mechanical displacement to further develop models of phonon−solvent interactions.

EXPERIMENTAL METHODS

Gold bipyramids and nanojavelins used in this study were both synthesized using a seed-mediated growth approach, but followed two separate synthesis routes published earlier.[16,27] Briefly, to synthesize gold bipyramids (samples A−E), gold seeds were created by reacting $HAuCl_4$ with $NaBH_4$ solution in the presence of sodium citrate. The seed was aged for 2 h before use. For growth of the bipyramid, $HAuCl_4$ solution with trace amount of $AgNO_3$ added were mixed with cetyltrimethylammonium bromide (CTAB) solution, acidified by a small amount of HCl, and reduced by L-ascorbic acid. Right after the reduction, small amounts of seeds were added, and the reaction was allowed to proceed in a 30 °C bath for 2 h. The aspect ratio of the bipyramid was controlled by the different amount of $AgNO_3$ added. Details information can be found in ref 16. To synthesize gold nanojavelins (samples F and G), seed was created by reduction of $HAuCl_4$ in the presence of 25% cetyltrimethylammonium chloride (CTAC) solution with $NaBH_4$/NaOH solution. The seeds were aged in a 85 °C oil bath for 1h, and further aged in ambient conditions for 1 day prior to the growth reaction. The growth solution consisted of $HACl_4$, a mixture of CTAB and CTAC, small amount of silver nitrate, and initiated by adding a mild reducing agent 8-hydroxyquinoline. Immediately after the reduction, different amounts of seeds are added to control the aspect ratio of nanojavelins. Further details appear in ref 27.

All samples were suspended in water for optical measurements and rapidly stirred. Transient absorption measurements were performed using a 2 kHz, 35 fs Ti:S amplifier. The 800 nm output was beamsplit to pump an optical parametric amplifier that produced tunable pump pulses at the LSPR of the sample, and a smaller portion was time-delayed and focused into sapphire to produce a white light probe beam. Pump pulses were mechanically chopped a 1 kHz to compare probe intensity though the sample with and without photoexcitation. Pump spot sizes were measured via transmission through a pinhole.

We performed finite-difference time-domain (FDTD, Lumerical Solutions) simulations to calculate the absorption and scattering spectra of the samples. We used a dielectric permittivity tabulated by Johnson and Christy for gold,[32] and the background refractive index was set to 1.33 for water. As the measurements have been performed on an assembly of bipyramids in solution, the calculated absorption spectra correspond to the sum of the spectral response under plane-wave irradiation with polarization parallel and perpendicular to the bipyramid long axis.

We also used FEA software (Abaqus, version 6.13−2) to calculate the frequency of the acoustic vibrations associated with each sample. These simulations have been performed on a continuous pentagonal bipyramid,[16] with material mechanical properties defined according to bulk gold (Young's modulus = 79 GPa, Poisson's ratio = 0.4, and density = 19300 $kg{\cdot}m^{-3}$). The modeling dimensions and shape (including length, width and radius of curvature) were based on the TEM measurement of several individual nanoparticle features.

ASSOCIATED CONTENT

Supporting Information

The Supporting Information is available free of charge on the ACS Publications website at DOI: 10.1021/acsphotonics.6b00136.

Additional information about the process of fitting the transient absorption data, discussion on phonon dephasing, explanation of how we minimized sample damage, table of particle dimensions, overall changes in particle size, cross sections from FDTD calculations (PDF).

AUTHOR INFORMATION

Corresponding Author

*E-mail: schaller@anl.gov; schaller@northwestern.edu.

Notes

The authors declare no competing financial interest.

ACKNOWLEDGMENTS

We acknowledge support from the Ultrafast Initiative of the U.S. Department of Energy, Office of Science, Office of Basic Energy Sciences, through Argonne National Laboratory under Contract No. DE-AC02-06CH11357. Use of the Center for Nanoscale Materials, an Office of Science user facility, was supported by the U.S. Department of Energy, Office of Science, Office of Basic Energy Sciences, under Contract No. DE-AC02-06CH11357.

REFERENCES

(1) Murray, W. A.; Barnes, W. L. Plasmonic materials. *Adv. Mater.* **2007**, *19*, 3771−3782.
(2) Stanley, R. Plasmonics in the mid-infrared. *Nat. Photonics* **2012**, *6*, 409−411.
(3) Knight, M. W.; King, N. S.; Liu, L.; Everitt, H. O.; Nordlander, P.; Halas, N. J. Aluminum for plasmonics. *ACS Nano* **2014**, *8*, 834−840.
(4) Hartland, G. V. Coherent vibrational motion in metal particles: Determination of the vibrational amplitude and excitation mechanism. *J. Chem. Phys.* **2002**, *116*, 8048−8055.
(5) Hartland, G. V. Optical Studies of Dynamics in Noble Metal Nanostructures. *Chem. Rev.* **2011**, *111*, 3858−3887.
(6) Link, S.; El-Sayed, M. A. Spectral Properties and Relaxation Dynamics of Surface Plasmon Electronic Oscillations in Gold and Silver Nanodots and Nanorods. *J. Phys. Chem. B* **1999**, *103*, 8410−8426.
(7) Willets, K. A.; Van Duyne, R. P. Localized Surface Plasmon Resonance Spectroscopy and Sensing. *Annu. Rev. Phys. Chem.* **2007**, *58*, 267−297.
(8) Fan, M.; Andrade, G. F. S.; Brolo, A. G. A review on the fabrication of substrates for surface enhanced Raman spectroscopy and their applications in analytical chemistry. *Anal. Chim. Acta* **2011**, *693*, 7−25.

DOI: 10.1021/acsphotonics.6b00136
ACS Photonics 2016, 3, 758−763

(9) Saha, K.; Agasti, S. S.; Kim, C.; Li, X.; Rotello, V. M. Gold Nanoparticles in Chemical and Biological Sensing. *Chem. Rev.* **2012**, *112*, 2739−2779.
(10) Vo-Dinh, T.; Wang, H. N.; Scaffidi, J. Plasmonic nanoprobes for SERS biosensing and bioimaging. *J. Biophoton.* **2010**, *3*, 89−102.
(11) Jain, P. K.; Huang, X.; El-Sayed, I. H.; El-Sayed, M. A. Noble metals on the nanoscale: optical and photothermal properties and some applications in imaging, sensing, biology, and medicine. *Acc. Chem. Res.* **2008**, *41*, 1578−1586.
(12) Hu, M.; Chen, J.; Li, Z.-Y.; Au, L.; Hartland, G. V.; Li, X.; Marquez, M.; Xia, Y. Gold nanostructures: engineering their plasmonic properties for biomedical applications. *Chem. Soc. Rev.* **2006**, *35*, 1084−1094.
(13) Bardhan, R.; Lal, S.; Joshi, A.; Halas, N. J. Theranostic Nanoshells: From Probe Design to Imaging and Treatment of Cancer. *Acc. Chem. Res.* **2011**, *44*, 936−946.
(14) Zhang, X.; Chen, Y. L.; Liu, R. S.; Tsai, D. P. Plasmonic photocatalysis. *Rep. Prog. Phys.* **2013**, *76*, 046401.
(15) Mukherjee, S.; Libisch, F.; Large, N.; Neumann, O.; Brown, L. V.; Cheng, J.; Lassiter, J. B.; Carter, E. A.; Nordlander, P.; Halas, N. J. Hot Electrons Do the Impossible: Plasmon-Induced Dissociation of H_2 on Au. *Nano Lett.* **2013**, *13*, 240−247.
(16) Liu, M.; Guyot-Sionnest, P. Mechanism of silver (I)-assisted growth of gold nanorods and bipyramids. *J. Phys. Chem. B* **2005**, *109*, 22192−22200.
(17) Pelton, M.; Sader, J. E.; Burgin, J.; Liu, M.; Guyot-Sionnest, P.; Gosztola, D. Damping of acoustic vibrations in gold nanoparticles. *Nat. Nanotechnol.* **2009**, *4*, 492−495.
(18) Pelton, M.; Wang, Y.; Gosztola, D.; Sader, J. E. Mechanical Damping of Longitudinal Acoustic Oscillations of Metal Nanoparticles in Solution. *J. Phys. Chem. C* **2011**, *115*, 23732−23740.
(19) Fernandes, B. D.; Spuch-Calvar, M.; Baida, H.; Tréguer-Delapierre, M.; Oberlé, J.; Langot, P.; Burgin, J. Acoustic Vibrations of Au Nano-Bipyramids and their Modification under Ag Deposition: a Perspective for the Development of Nanobalances. *ACS Nano* **2013**, *7*, 7630−7639.
(20) Major, T. A.; Lo, S. S.; Yu, K.; Hartland, G. V. Time-resolved studies of the acoustic vibrational modes of metal and semiconductor nano-objects. *J. Phys. Chem. Lett.* **2014**, *5*, 866−874.
(21) van Dijk, M. A.; Lippitz, M.; Orrit, M. Detection of Acoustic Oscillations of Single Gold Nanospheres by Time-Resolved Interferometry. *Phys. Rev. Lett.* **2005**, *95*, 267406.
(22) Hartland, G. V. Ultrafast studies of single semiconductor and metal nanostructures through transient absorption microscopy. *Chem. Sci.* **2010**, *1*, 303−309.
(23) Ruijgrok, P. V.; Zijlstra, P.; Tchebotareva, A. L.; Orrit, M. Damping of Acoustic Vibrations of Single Gold Nanoparticles Optically Trapped in Water. *Nano Lett.* **2012**, *12*, 1063−1069.
(24) Plech, A.; Kotaidis, V.; Grésillon, S.; Dahmen, C.; von Plessen, G. Laser-induced heating and melting of gold nanoparticles studied by time-resolved x-ray scattering. *Phys. Rev. B: Condens. Matter Mater. Phys.* **2004**, *70*, 195423.
(25) Clark, J. N.; Beitra, L.; Xiong, G.; Higginbotham, A.; Fritz, D. M.; Lemke, H. T.; Zhu, D.; Chollet, M.; Williams, G. J.; Messerschimdt, M.; Abbey, B.; Harder, R. J.; Korsunsky, A. M.; Wark, J. S.; Robinson, I. K. Ultrafast Three-Dimensional Imaging of Lattice Dynamics in Individual Gold Nanocrystals. *Science* **2013**, *341*, 56−59.
(26) Lee, J.-H.; Gibson, K. J.; Chen, G.; Weizmann, Y. Bipyramid-templated synthesis of monodisperse anisotropic gold nanocrystals. *Nat. Commun.* **2015**, *6*, 7571.
(27) Chateau, D.; Liotta, A.; Vadcard, F.; Navarro, J. R. G.; Chaput, F.; Lermé, J.; Lerouge, F.; Parola, S. From gold nanobipyramids to nanojavelins for a precise tuning of the plasmon resonance to the infrared wavelengths: experimental and theoretical aspects. *Nanoscale* **2015**, *7*, 1934−1943.
(28) Liu, M.; Guyot-Sionnest, P.; Lee, T. W.; Gray, S. K. Optical properties of rodlike and bipyramidal gold nanoparticles from three-dimensional computations. *Phys. Rev. B: Condens. Matter Mater. Phys.* **2007**, *76*, 235428.
(29) Knünz, S.; Herrmann, M.; Batteiger, V.; Saathoff, G.; Hänsch, T. W.; Vahala, K.; Udem, Th. Injection Locking of a Trapped-Ion Phonon Laser. *Phys. Rev. Lett.* **2010**, *105*, 013004.
(30) Crut, A.; Juvé, V.; Mongin, D.; Maioli, P.; Del Fatti, N.; Vallée, F. Vibrations of Spherical Core-Shell Nanoparticles. *Phys. Rev. B: Condens. Matter Mater. Phys.* **2011**, *83*, 205430.
(31) Major, T. A.; Crut, A.; Gao, B.; Lo, S. S.; Del Fatti, N.; Vallée, F.; Hartland, G. V. Damping of the Acoustic Vibrations of a Suspended Gold Nanowire in Air and Water Environments. *Phys. Chem. Chem. Phys.* **2013**, *15*, 4169−4176.
(32) Johnson, P. B.; Christy, R. W. Optical Constants of the Nobel Metals. *Phys. Rev. B* **1972**, *6*, 4370−4379.

DOI: 10.1021/acsphotonics.6b00136
ACS Photonics 2016, 3, 758−763